



LAWRENCE
LIVERMORE
NATIONAL
LABORATORY

Qualification of Automated Low-Field NMR Relaxometry for Quality Control of Polymers in a Production Setting

S.C. Chinn, A. Cook-Tendulkar, R.S. Maxwell, H.
Wheeler, M. Wilson, Z.H. Xie

June 16, 2007

Polymer Testing

Disclaimer

This document was prepared as an account of work sponsored by an agency of the United States Government. Neither the United States Government nor the University of California nor any of their employees, makes any warranty, express or implied, or assumes any legal liability or responsibility for the accuracy, completeness, or usefulness of any information, apparatus, product, or process disclosed, or represents that its use would not infringe privately owned rights. Reference herein to any specific commercial product, process, or service by trade name, trademark, manufacturer, or otherwise, does not necessarily constitute or imply its endorsement, recommendation, or favoring by the United States Government or the University of California. The views and opinions of authors expressed herein do not necessarily state or reflect those of the United States Government or the University of California, and shall not be used for advertising or product endorsement purposes.

Qualification of Automated Low-Field NMR Relaxometry for Quality Control of Polymers in a Production Setting

Sarah C. Chinn*, Angela Cook-Tendulkar, Robert Maxwell
Lawrence Livermore National Laboratory
7000 East Ave, Livermore, CA 94550

Hilary Wheeler, Mark Wilson
Honeywell Federal Manufacturing & Technologies, Kansas City Plant,
Kansas City, MO 64141

Z. Harry Xie
Bruker Optics, minispec Division, The Woodlands, TX 77381

Abstract

Implementation of a low field time-domain NMR scanner as a diagnostic tool in the production of new polymer components is described in the context of qualification of a new QA/QC device. A study to determine the optimal experimental parameters was performed and a robotic autosampler was built to enable scanning of multiple pads. Relationships between T_2 values and physical properties of DC745 slabs were investigated, and the appropriate sampling parameters for the production setting were determined. Two versions of a robotic autosampler were built, and for the component described here a fourth radial axis was required in addition to traditional X, Y, and Z movement to eliminate the large variability in T_2 due to inconsistent sample coverage caused by complex rib geometry of the component. Data show that with appropriate choice of experimental conditions of the NMR detector and the detection geometry of the

robotic autosampler, sufficient resolution of variations in crosslink density on the millimeter scale could be determined. All data to date demonstrates that low-field NMR devices are a feasible tool for use in production settings for non-destructive quality control of polymer components.

Keywords: NMR, polymer testing, quality control, PDMS, TD-NMR, crosslink

* Corresponding author: Email: chinn7@llnl.gov; Phone: 925-422-5514

1. Introduction:

Nuclear magnetic resonance (NMR) spectroscopy is routinely used to investigate structural and dynamic properties of polymers [1] and has found extensive use in investigating the effects of long-term exposure to chemically, thermally, or radioactively harsh environments on polymeric materials. [2-7] In the last decade, low-field, single sided time-domain NMR experiments using equipment such as the NMR MOUSE^{®1} or the Bruker minispec ProFiler have become popular in the area of material characterization. Numerous applications of low-field relaxometry for non-destructive testing of polymers have been reported. [8-12] Much of the recent work in the area of low-field NMR has been to develop novel NMR pulse sequences to enhance the amount and resolution of the NMR information available from the system. For example, work has been done using Ex-Situ NMR techniques [13] to obtain liquid-like NMR spectra from a single-sided magnet. [14,15] Additional efforts have been made in the areas of multiple quantum NMR, [16,17] low-power selective excitation, [18,19] and numerous magnetic resonance imaging (MRI) applications. [20-22] Recent incorporation of a 1D adjustable magnet stage using the Profile NMR-MOUSE[®] has allowed for depth profiling within a sample. Modifications to the magnet system as well as the ability to make minute changes in the distance between the magnet surface and the sample has afforded very high resolution depth profiles on the order of $\sim 2 \mu\text{m}$. [23]

In cases of elastomer degradation, low field instruments have been able to reproducibly detect polymer deformation, [11,12] increased crosslinking due to aging or to manufacturing imperfections, [24-26] or detect defects in large materials such as

¹ NMR-MOUSE[®] is a registered trademark of RWTH-Aachen, Germany

vehicle tires. Much of the time, the handheld magnet unit can be held up to the surface of the polymer part for analysis, or the test coupon can be placed directly on the magnet face. For some specific applications, a custom magnet unit has been built to match the geometry of the part. [8,11] However, in certain applications where testing of numerous large parts requires accurate test patterns to provide higher resolution testing, a hand-held sensor becomes inefficient. Here we present a combination of a robotic autosampler with low-field NMR spectroscopy for applications of quality control of elastomers. The autosampler allows 3-dimensional testing capabilities along with a rotational axis to allow for a reproducible test footprint for components that possess a unique radial geometry.

It has recently been shown that low-field time-domain NMR can be used to detect chemical changes in the deformed sections of damaged components made from a PDMS-based polymer called DC745 via changes in the T_2 relaxation time. [12] These changes can be rendered two-dimensionally via T_2 -weighted magnetic resonance images, and it has been shown that high resolution is not necessary for macroscopic defects. [12] In fact, it was shown that low-field NMR could be a valuable tool in the production of new polymer parts by screening new pads and identifying potentially defective pads, since the defects are thought to originate from inhomogeneities in the initial mixing process during component production. Fine control of the experimental parameters used in the analysis can be used to optimize the sensitivity of the measurement, [9,27] essentially tailoring the diagnostic specifically to the test sample. However, in most quality control and production settings, thorough evaluation and qualification of the test methods are often required, though detailed optimization of the parameters is not feasible due to time

constraints or lack of NMR experience by the production or QA/QC engineer. In this paper we identify the necessary experimental variables that must be considered by a novice technician in optimizing the low-field NMR test method and introduce the automation capability for non-destructive screening of multiple polymer production parts, significantly reducing the need for human interaction.

2. Experimental:

Low field time-domain NMR relaxometry uses the same principles of traditional NMR spectroscopy, but since only relaxation information is obtained, the normal high resolution that is typically required for complete structural analysis is not needed. In the application of NMR relaxometry used here, the initial rf pulse is applied followed by a separate train of pulses that refocuses the magnetization into a series of “echoes”. The intensity of the echoes decays in time with a time constant T_2 as the magnetization is transferred to neighboring spins as a result of internal motion of the polymer network. Detailed analysis of the relationship between T_2 relaxation time and polymer dynamics has been described elsewhere. [1,28]

The Bruker minispec ProFiler, used in this study, consists of a computer, tabletop spectrometer console and preamplifier, and a magnet unit. The magnet unit consists of two permanent magnets with anti-parallel magnetization producing a B_0 field parallel to the surface of the unit, as shown in Fig. 1. B_1 irradiation is applied with a surface rf coil in the center producing a smaller magnetic field perpendicular to the surface. The magnet unit can be held by hand or by a robotic controller and scanned systematically over the entire surface of the polymer component. The spatial resolution is

approximately 1.5 cm^2 , about the width of two ribs, which is of comparable size to the deformed areas of the pads.

2.1 Sample preparation

DC745 was obtained from Dow Corning as Silastic[®] 745U and crosslinked with 0.55 wt% peroxide curing agent. Samples were cured from Dow Corning 745U silicone cured with 2,5-dimethyl-2,5-di(t-butylperoxy)hexane peroxide curing agent supported on CaCO_3 . Curing was performed by thermal activation at $170 \text{ }^\circ\text{C}$ for ten minutes. DC745 also contains ~30 wt.% mixture of quartz and high surface area reinforcing fumed silica fillers and small amounts of CaCO_3 remaining from the curing agent. A number of components which were deformed during their service life were tested in addition to newly produced components. Samples for the experiments and instrument qualification presented here were intact polymer pads either placed on top of the magnet unit or placed on a table with the magnet unit lowered to the component surface.

2.2 Low field time domain NMR experiments

Static, uniaxial NMR relaxation times were measured using the Carr-Purcell-Meiboom-Gill (CPMG) [29] pulse sequence on a Bruker minispec ProFiler from Bruker Optics operating at 16 MHz. Unless otherwise indicated, the experimental parameters were set as follows: 128 scans, 600 echoes, and 0.5 ms echo time. These parameters were optimized as described below for ideal production settings. The echo times were systematically increased until the T_2 remained consistent to avoid the interfering spin-locking effects of $T_{1\rho}$ in the CPMG experiment. The pulse attenuation, receiver gain, and

recycle delay were set to 6 dB, 103 dB, and 1 s, respectively, unless otherwise indicated.

Decay curves were fit to a two-component exponential decay

$$E(t) = A_1 \exp\left(-\frac{t}{T_{2_1}}\right) + A_2 \exp\left(-\frac{t}{T_{2_2}}\right) \quad (1)$$

using the Bruker software.

2.3 Automated robotic autosampler

The automated robotic system was developed joint with Bruker Optics, Inc., Minispec Division (The Woodlands, TX). The magnet of the NMR ProFiler, also called the NMR sensor, was mounted to a modified commercial Autosampler (Duratech, Waynesboro, VA) for automated NMR experiments (Figure 5). The Autosampler is a three-axis (XYZ) gantry-type robot. Each axis is controlled through Bruker minispec software. A special glass platform with 6 sample locating PTFE discs is used to accommodate up to 6 polymer sample pads for one session of analysis. Each sample pad is scanned by the automated NMR sensor according to a pre-defined scan pattern to obtain the NMR T_2 relaxation time. An advanced version of the automation system was developed for this study to include the rotational control of the NMR sensor so that each scanned spot can be described by X,Y (the location on the pad), Z (the vertical height or the thickness of the pad) and W (the NMR sensor rotational orientation). A 7th sample position is available for irregularly shaped samples. Coordination and orientation information of each scan together with NMR measurement parameters and relaxation time results are logged into a spreadsheet during the automated measurement. The results can then be easily utilized for further data analysis.

3. Results & Discussion:

An initial investigation of the applicability of low-field NMR has been published previously. [12] In short, it was determined that the ProFiler was able to distinguish between damaged and undamaged sections from a damaged part in a nondestructive fashion. Fig. 2 shows an image of the damaged section and the corresponding difference in T_2 relaxation time. Here, a difference of ~ 20 ms was observed between the damaged and undamaged section of the damaged component, demonstrating that the damage is easily discernable with the NMR ProFiler.

3.1 Determination of Optimal Experimental Parameters

Additional studies were performed to determine the amount of variability of the ProFiler measurements from the same section of a pad. A section of the polymer pad was placed on the NMR ProFiler for inspection and the scan was performed ten separate times. The pad was not moved or disturbed in any way between these consecutive tests. The average variability in the measurement was shown to be 3.22%, which was assumed to be acceptable since, as seen above, the expected decrease in T_2 relaxation time between the damaged and undamaged sections was roughly 20%.

Though the data obtained from the same spot on a pad displayed adequate reproducibility, a larger discrepancy was observed while measuring different pads or different sections of the same pad. One potential source for the scatter was considered to be the effect of varying signal to noise ratios between different measured sections. As the signal intensity or sensitivity of the NMR detection increases by either signal averaging

or detecting a larger sample volume, the echo decay curve measured by the NMR ProFiler displays less scatter and a more accurate fit to an exponential decay curve is obtained. Alternatively, if the noise level of the measurement increases, the decay curve shows more scatter and the data does not fit as well to an exponential decay. Both of these circumstances were considered by varying the number of scans to investigate the effect of signal to noise on the T_2 time and repeating these measurements after placing the NMR ProFiler inside an aluminum box to eliminate noise from external sources. The results, shown in Fig. 3, show that the T_2 indeed increases with increasing number of scans, though in this case the effect of the shielding box was negligible. [Note that one data point was eliminated in the 512 scan, with shield plot due to an errant measurement.] It was determined that efforts must be taken to ensure that the S/N ratio of each measurement is similar to produce appropriate T_2 measurements across a single pad or between pads.

Finally, the number of echoes and the delay time between echoes were optimized to provide the highest signal intensity while avoiding losing data at the tail end of the decay curve. As mentioned in the experimental section, the CPMG experiment proceeds via a 90° pulse followed by a series of 180° pulses which refocus the magnetization into a series of echoes. The time between 180° pulses in the echo train and the number of pulses determines the overall length of the NMR experiment. The optimal decay curve would result in a complete decay after six time constants have elapsed. Too few echoes or echo times which are too short result in incomplete decay and lost data, as shown in Fig. 4(a). Conversely, if the echo time is too long or too many echoes are obtained, the curve would decay too fast, resulting in a less accurate fit to the decay curve due to the

abundance of signal from the noise itself, as evidenced in Fig. 4(b). The optimal parameters for the material in this study were determined to be an echo time of 0.5 ms and acquisition of 600 echoes, as determined by the decay curve which decayed to zero in six time constants in Fig. 4(c). It was determined that these parameters would be used in all subsequent measurements of this material.

3.2 Robotics and Autosampler:

In order to reduce the opportunities for human error and reduce the amount of time needed to physically operate the NMR ProFiler in a production setting, a robotic autosampler was developed. This automatic inspection system was developed in collaboration with Bruker Optics, Inc. and is shown in Fig. 5. The autosampler was designed to measure six DC745 components automatically without the need for human interaction. The original design included a triple axis robotic arm that held the ProFiler magnet unit and lowered it down onto the pad and moved it in a pre-programmed pattern around the entire pad, sampling each section of the pad. After an entire pad was scanned, the ProFiler moved onto the surface of the next pad and continued until all six pads had been scanned.

Initial tests were performed using the robotic autosampler to determine if a damaged section of a pad could be distinguished. Using the intended sampling pattern which took advantage of the three-axis robotic arm, a large amount of scatter or variance was observed across each pad. As demonstrated in Fig. 6, the expected difference of roughly 20 ms in T_2 value between the damaged and undamaged section of the pad was within the variance of the measurement, so the damaged sections could not be observed.

In this case the large variance in the data was assumed to be due to the complex rib geometry of the DC745 component and the result that the magnet unit is sampling both the polymer material and the air gaps between the ribs. The significant difference in magnetic susceptibility between air and the polymer drastically changes the T_2 measurement. It was determined that the rib geometry led to inconsistent coverage by the three-dimensional robotic movement of the ProFiler magnet unit, as demonstrated in Fig. 7(a). As the ProFiler unit moved to different sections of the pad, the total detection volume contained a different overall volume of the sample. However, by adding a fourth axis in a radial dimension, the same amount of polymer and air in the active volume of the surface coil of the magnet could be detected all around the pad, as demonstrated in Fig. 7(b). The ideal design would allow the magnet itself to rotate as demonstrated in Figure 7(c) such that the total coverage was the same for every position on the component. In an initial trial to simulate the effects of the fourth axis, the magnet unit remained in the same x and y position, raised in the z dimension slightly, the pad was rotated underneath the magnet, and the magnet lowered to the surface. Using this method a visible decrease in variance in the T_2 measurements was observed, and the expected ~20 ms drop in T_2 was clearly observed in a section where damage was visible to the eye, as shown in Fig. 8. While the example shown in Fig. 8 was a rough measurement with only a few data points, it is clear that the addition of the radial axis would yield an observable difference between damaged and undamaged sections of the component.

With the ultimate goal of eliminating defective parts from going into service, a number of new components were tested. Fig. 9 shows the results of scanning fifteen pads using the 4-axis autosampler. In the individual value plot shown here, each T_2 value

measured around the pad was plotted on the same corresponding x-axis point representing each pad, showing the distribution of T_2 values on each individual part. It is obvious that one pad showed potential defect sites due to the outlying data points roughly 20 ms lower than the majority of the points, while several additional pads displayed outlying data points roughly 10 ms lower than the rest. It is uncertain whether these sites would eventually lead to deformation after an extended time in service, and more investigation is needed in this area. The individual points are plotted as a function of position in Fig. 10(a), with position 1 being the top, 0 degree position on the circular part and each additional point is taken every 25 degrees, with finer sampling increments being used in areas of particular interest. The red and black points are two scans over the same region to demonstrate the reproducibility. The plot clearly shows an area between points 7 and 9 with a 20 ms decrease in T_2 , indicate a potential defect site. In the case of this polymer component, it was not possible to test the pad to see if the deformation would form, but Shore M hardness tests were performed and indeed revealed a decrease in hardness in the area identified by the low field NMR minispec ProFiler. A comparison between the T_2 results and the Shore M hardness results is shown in Fig. 10(b). Finally, upon highly detailed visual inspection, it was determined that a void was present in the material, which would ultimately lead to the decrease in hardness and permanent deformation of the material. The void was not observed during the routine visual inspection performed as part of the acceptance testing of the component. This clearly demonstrates an inhomogeneity in the production process leading to defects unobservable to the naked eye and identifies the usefulness of low-field NMR in a production setting.

4. Conclusions

The NMR ProFiler is a benchtop NMR spectrometer that can be used to perform relaxation measurements on intact polymer parts. A detailed investigation into the optimal experimental parameters for use as a QA/QC tool in the production of new polymer components has been performed. For the component studied here, the appropriate sampling parameters for the production setting was determined to be 128 scans, 600 echoes, and 0.5 ms echo time. A three-axis robotics system was built and tested for measurement reproducibility, though the inconsistent coverage of the NMR sensor due to the complex rib geometry of the components led to a large amount of scatter in the measurement. A fourth radial dimension was added to allow the sensor to rotate to match the curvature of the component, which successfully eliminated the large variability in T_2 due to inconsistent sample coverage. The low-field NMR ProFiler has been successful in identifying potentially problematic polymer components, suggesting that low-field NMR devices are a feasible tool for use in production settings for non-destructive quality control of polymer components.

Acknowledgements

This work was performed under the auspices of the U.S. Department of Energy by U. C., Lawrence Livermore National Laboratory under contract # W-7405-Eng-48.

References:

1. K. Schmidt-Rohr, H. W. Spiess. *Multidimensional Solid State NMR and Polymers*; San Diego: Academic Press, 1994.
2. A. Charlesby. *Radiation Effects in Macromolecules: Their Determination with Pulsed Nuclear Magnetic Resonance (NMR)*. *Rad. Phys. Chem.* 1985; 26: 463.

3. A. Chien, R. S. Maxwell, D. Chambers, B. Balazs, J. LeMay. Characterization or radiation-induced aging in silica-reinforced polysiloxane composites. *J. Rad. Phys. Chem* 2000; 59: 493.
4. R. Maxwell, B. Balazs. Residual dipolar coupling for the assessment of crosslink density changes in γ -irradiated silica-PDMS composite materials. *J. Chem. Phys.* 2002; 116: 10492.
5. R. Maxwell, B. Balazs. NMR measurements of residual dipolar couplings for lifetime assessments in γ -irradiated silica-PDMS composite materials. *Nuc. Inst. Meth. Phys. Res. B* 2003; 208: 199.
6. R. Maxwell, R. Cohenour, W. Sung, D. Solyom, M. Patel. The effects of γ -irradiation on the thermal, mechanical, and segmental dynamics of a silica filled, room temperature, vulcanized polysiloxane rubber. *Poly. Deg. Stab.* 2003; 80: 443.
7. R. S. Maxwell, S. C. Chinn, D. Solyom, R. Cohenour. Radiation induced degradation in a silica-filled silicone elastomer as investigated by multiple quantum NMR. *Macromolecules* 2005; 38: 7026.
8. H. Kuhn, M. Klein, A. Wiesmath, D. E. Demco, B. Blümich, J. Kelm, P. W. Gold. The NMR-MOUSE(R): quality control of elastomers. *Magnetic Resonance Imaging* 2001; 19: 497.
9. A. Guthausen, G. Zimmer, P. Blümmler, B. Blümich. Analysis of polymer materials by surface NMR via the MOUSE. *Journal of Magnetic Resonance* 1998; 130: 1.
10. V. Herrmann, K. Unseld, H. B. Fuchs, B. Blümich. Molecular dynamics of elastomers investigated by DMTA and the NMR-MOUSE(R). *Colloid & Polymer Science* 2002; 280: 758.
11. B. Blümich, F. Casanova, A. Buda, K. Kremer, T. Wegener. Mobile NMR for Analysis of Polyethylene Pipes. *Acta Physica Polonica A* 2005; 108: 13.
12. J. L. Herberg, S. C. Chinn, A. M. Sawvel, E. Gjersing, R. S. Maxwell. Characterization of local deformation in filled-silicone elastomers subject to high strain - NMR MOUSE and Magnetic Resonance Imaging as a diagnostic tool for detection of inhomogeneities. *Poly. Degrad. Stab.* 2006; 91: 1701.
13. C. Meriles, D. Sakellariou, H. Heise, A. J. Moule, A. Pines. Approaches to high resolution ex-situ spectroscopy. *Science* 2001; 293: 82.
14. J. Perlo, F. Casanova, B. Blümich. Ex-situ NMR in highly homogeneous fields; ^1H spectroscopy. *Science* 2007; 315: 1110.
15. J. Perlo, V. Demas, F. Casanova, C. Meriles, J. Reimer, A. Pines, B. Blümich. High resolution spectroscopy with a portable single-sided sensor. *Science* 2005; 308: 1279.
16. A. Wiesmath, C. Filip, D. E. Demco, B. Blümich. Double-quantum-filtered NMR signals in inhomogeneous magnetic fields. *Journal of Magnetic Resonance* 2001; 149: 258.
17. A. Wiesmath, C. Filip, D. E. Demco, B. Blümich. NMR of multipolar spin states excited in strongly inhomogeneous magnetic fields. *Journal of Magnetic Resonance* 2002; 154: 60.
18. M. Todica, R. Fechete, B. Blümich. Selective NMR excitation in strongly inhomogeneous magnetic fields. *Journal of Magnetic Resonance* 2003; 164: 220.

19. M. Todica, B. Blümich. Optimization of the DANTE pulse sequence for selective NMR excitation in strongly inhomogeneous magnetic fields. *Int. J. of Mod. Phys.* 2004; 18: 1571.
20. G. Navon, U. Eliav, D. E. Demco, B. Blümich. Study of the order and dynamic processes in tendon by NMR and MRI. *J. Mag. Reson. Imag.* 2007; 25: 362.
21. S. Ahola, J. Perlo, F. Casanova, S. Stapf, B. Blümich. Multiecho sequence for velocity imaging in inhomogeneous rf fields. *J. Magn. Reson.* 2006; 182: 143.
22. J. Perlo, F. Casanova, B. Blümich. Velocity imaging by ex situ NMR. *Journal of Magnetic Resonance* 2005; 173: 254.
23. J. Perlo, F. Casanova, B. Blümich. Profiles with microscopic resolution by single-sided NMR. *Journal of Magnetic Resonance* 2005; 176: 64.
24. S. C. Chinn, S. DeTeresa, A. Shields, A. M. Sawvel, B. Balazs, R. S. Maxwell. Chemical origins of permanent set in a peroxide cured filled silicone elastomer - tensile and ^1H NMR analysis. submitted to *Poly. Degrad. Stab.* 2004.
25. G. Zimmer, A. Guthausen, B. Blümich. Characterization of cross-link density in technical elastomers by the NMR-MOUSE. *Solid State Nuclear Magnetic Resonance* 1998; 12: 183.
26. S. Anferova, V. Anferov, M. Adams, R. Fehete, G. Schroeder, B. Blümich. Thermo-oxidative aging of elastomers: a temperature control unit for operation with the NMR-MOUSE. *Appl. Magn. Reson.* 2005; 27: 1.
27. B. Blümich, F. Casanova, J. Perlo, S. Anferova, V. Anferov, K. Kremer, N. Goga, K. Kupferschlager, M. Adams. Advances of unilateral mobile NMR in nondestructive materials testing. *Magnetic Resonance Imaging* 2005; 23: 197.
28. J. P. Cohen-Addad. NMR and fractal properties of polymer liquids and gels. *Prog. NMR Spect.* 1993; 25: 1.
29. S. Meiboom, D. Gill. Modified spin-echo method for measuring nuclear relaxation times. *Rev. Sci. Instr.* 1958; 29: 688.

Figure Captions:

Fig. 1. Photo and schematic of ProFiler magnet unit, showing the B_0 (black dashed) and B_1 (red dashed) magnetic field lines and the DC745 sample (dark grey).

Fig. 2. Photo of damaged and undamaged spots from damaged DC745 component with corresponding T_2 relaxation times.

Fig. 3. Effect of number of scans and effects of noise shield.

Fig. 4. Effect of varying echo time and number of echos on the relaxation curve. Optimal curves should be fully decayed in after 6 time constants, indicated by vertical lines in the plots.

Fig. 5. Photo of Robotic Autosampler designed by Bruker Optics, Inc.

Fig. 6. Large amount of scatter in damaged component observed using 3-axis robotics system. The red circle indicates the area of visible damage on the pad.

Fig. 7. Active detection volume of NMR sensor with a 3-axis (a) and 4-axis (b) robotic autosampler, and (c) demonstration of rotation of NMR sensor.

Fig. 8. NMR ProFiler scan from damaged pad using 3-axis autosampler and physically rotating the component to simulate 4th rotational axis.

Fig. 9. Individual value plot of fifteen new production parts obtained with advanced, 4-axis robotic autosampler.

Fig. 10. (a) Scan from new pad showing potentially damaged area using advanced 4-axis robotic autosampler and (b) comparison of low-field NMR results to Shore M hardness tests.

Fig. 1

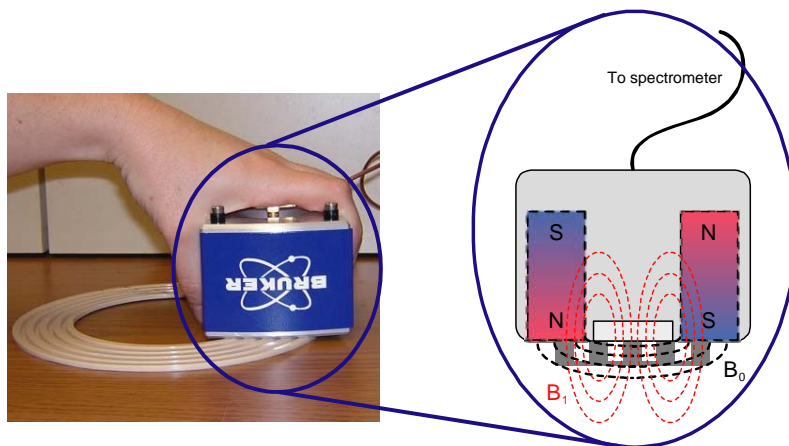


Fig. 2

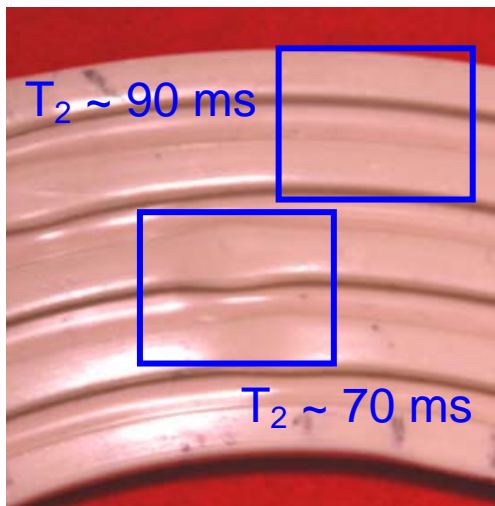


Fig. 3

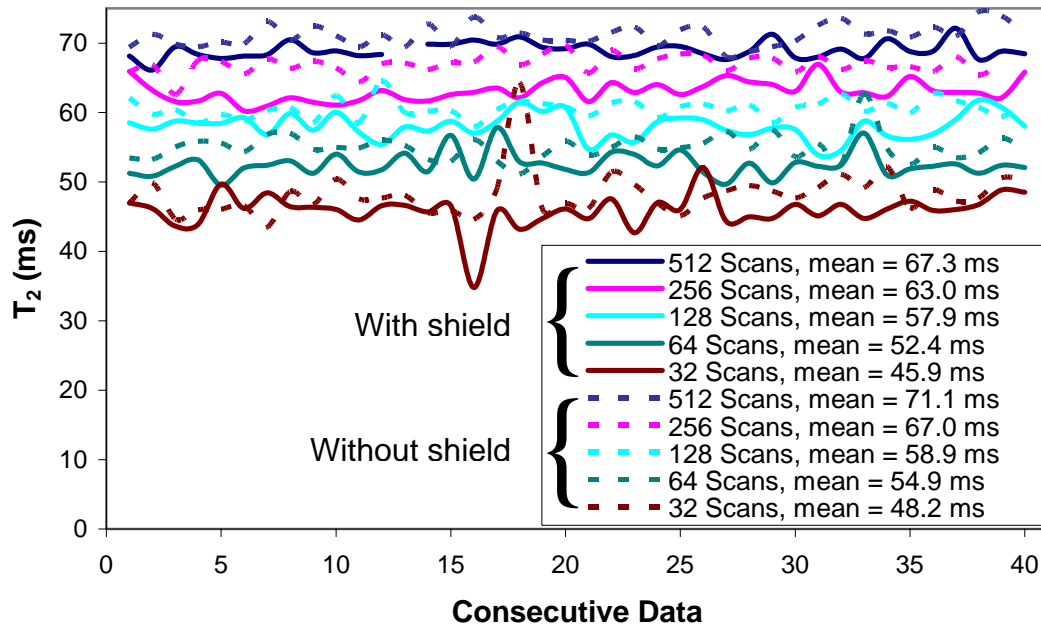


Fig. 4

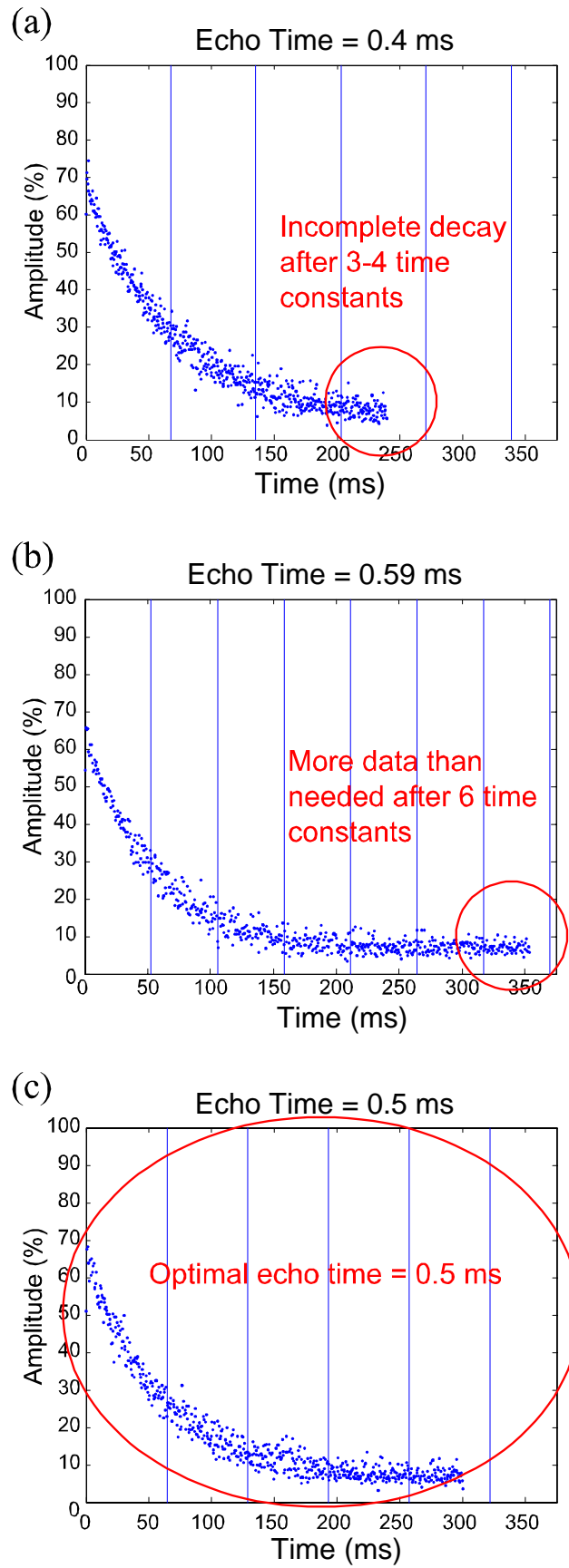


Fig. 5



Fig. 6

Damaged pad, 3-axis robotic autosampler

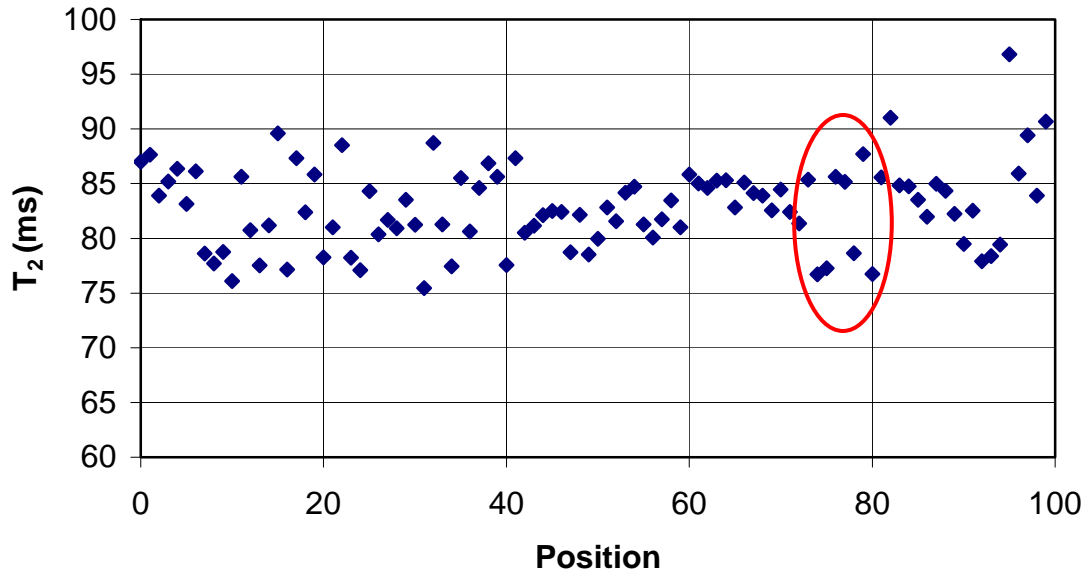


Fig. 7

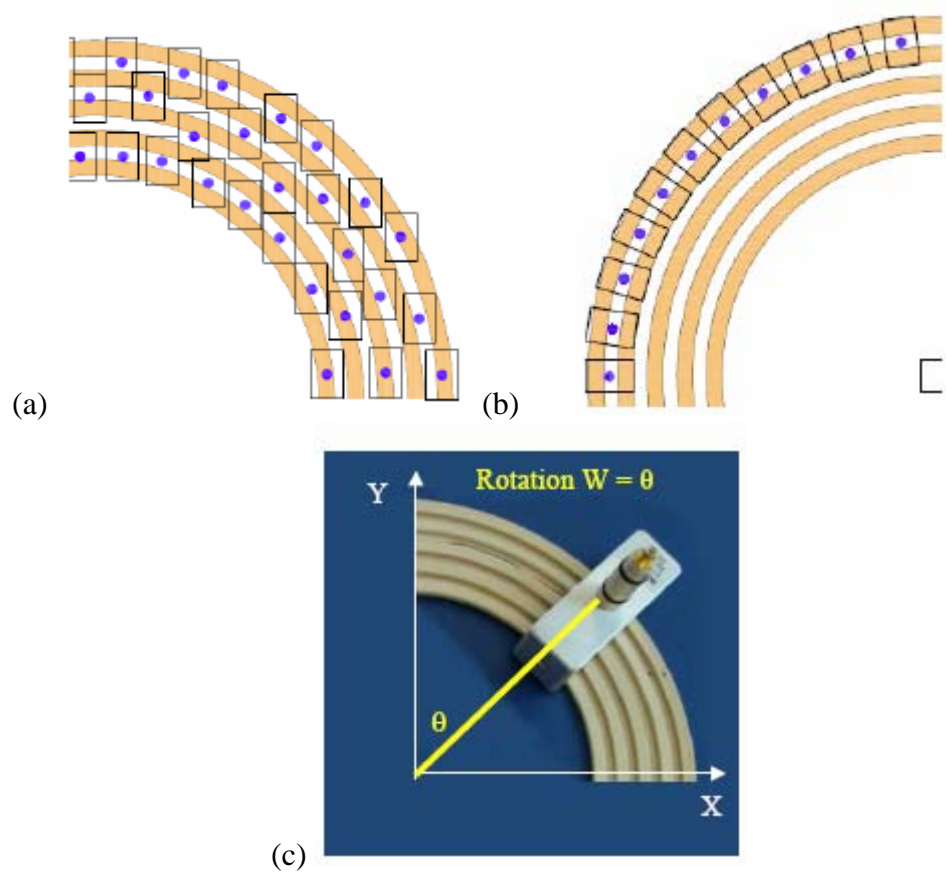


Fig. 8

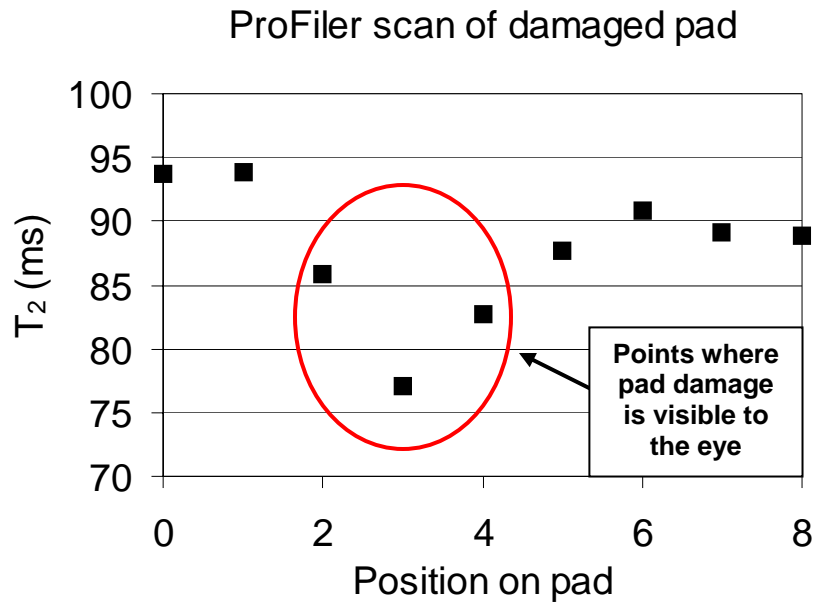


Fig. 9

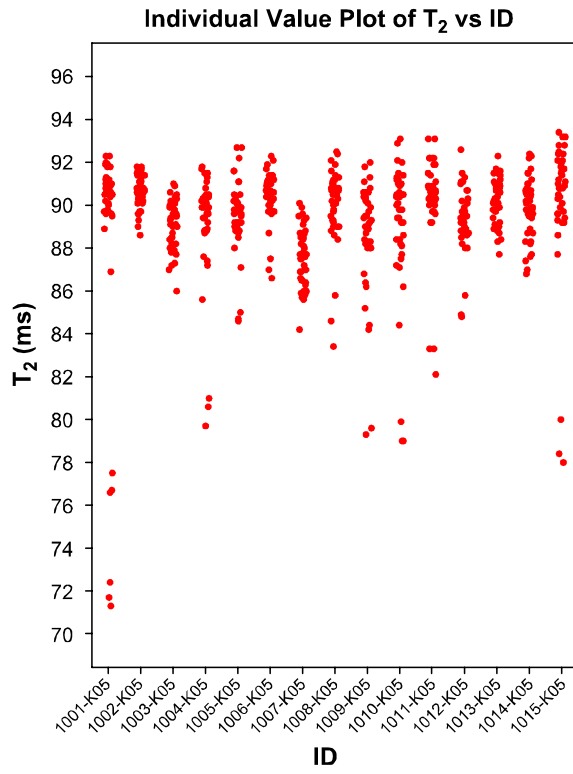


Fig. 10

